Influence of backflow on the reorientation dynamics of ferroelectric liquid crystals

Zhong Zou and Noel A. Clark
Department of Physics, Condensed Matter Laboratory, and Center for Optoelectronic Computing Systems, University of Colorado, Boulder, Colorado 80309

Tomas Carlsson
Physics Department, Chalmers University of Technology, S-412 96 Göteborg, Sweden
(Received 14 May 1993)

The elasto hydrodynamic equations for coupled reorientation and flow in surface-stabilized ferroelectric liquid-crystal cells have been solved numerically and the results are compared to the case in which the flow effects are neglected. Our simulations show that flow generally makes the switching faster in the case of the dipoles being in an unstable equilibrium state in an applied field. Our calculations show that it is important to include the backflow in the reorientation dynamics in order to have the correct switching picture.

PACS number(s): 61.30.−v

I. INTRODUCTION

The coupling of molecular orientation to flow plays an important role in the response of nematic liquid crystals to an applied field. Thus molecular reorientation can generate a flow which can in turn affect the reorientation. In ferroelectric liquid crystals, since director reorientation is much more rapid than in nematics, it might be expected that flow effects are correspondingly more important. In this paper we show that this is in fact the case.

The equations describing the coupling between orientational motion of the director and mass flow have been developed for nematics by Ericksen [1] and Leslie [2] and solved numerically for twisted nematic cells by van Doorn [3] and Berremann [4]. Since the surface-stabilized ferroelectric liquid crystal (SSFLC) cell was invented [5], there have been intensive studies of its director dynamics. However, there are none to date in which coupling to flow is taken into consideration. However, the experiments with nematic liquid crystals and the electromechanical experiments of Jakli and Saupe [6,7] suggest that coupling of director reorientation and flow may be important in SSFLC cells. Jakli's experiments have shown that switching in a SSFLC cell can produce mechanical motion of the bounding plates in cells where relative motion of the plates is possible. Recently, Jakli and Saupe have suggested backflow as a possible origin of the mechanical motion [7].

In this paper we study in which way the reorientational motion of the director is affected by taking the coupling between director rotations and mass flow in the system into account. Since the hydrodynamic theory of smectic-C (Sm-C^*) liquid crystals has not been available until recently [8,9], all the previous studies of the switching dynamics of SSFLC cells are based on the equations for which the mass flow in the system has been neglected. For instance, when solving the switching equation while ignoring the flow effect on the molecular orientation, Maclennan, Handschy, and Clark [10] show that there can be a beautiful solitary wave traveling across SSFLC cells when the sign of a strong applied field is changed. (This result is also shown in row 1 of Fig. 4 of this paper and compared with the result for which backflow effects are taken into account.) However, there has not yet been reported any conclusive experimental evidence which supports the long switching times associated with solitary-wave propagation in the cell geometry described in Ref. [10], although somewhat longer switching times are found for field reversal relative to those for switching from a relaxed state [11]. This may suggest that, as in nematic liquid crystals, the flow effects should not be neglected for a complete (or correct) picture of switching dynamics. It is also likely that the coupling to flow may be responsible for the speedy boat shape of switching domains in chevron cells [12].

In this paper we will limit our discussion to the bookshelf cell and leave the more complicated chevron case to a future publication. In this work, the flow-coupled switching equations in SSFLC cells are solved numerically. In Sec. II we present the formalism and the computation method. The equations governing the dynamic behavior of the system used here are derived via the viscoelastic theory of Sm-C and Sm-C^* liquid crystals by Leslie and co-workers [8,9,13] as a starting point. The derivation of the governing equations will be published elsewhere [14]. In Sec. III the numerical solutions to these coupled nonlinear partial differential equations for various fixed boundary conditions are presented and compared to the results from the dynamic equations which do not contain flow terms. Finally, we summarize our results and discuss their physical implications in Sec. IV.

II. THEORETICAL BACKGROUND AND COMPUTATION SCHEME

For simplicity, a bookshelf geometry SSFLC cell is assumed. Our choice of coordinates is shown in Fig. 1. The substrate normal is taken to coincide with $\hat{\mathbf{x}}$, while $\hat{\mathbf{z}}$

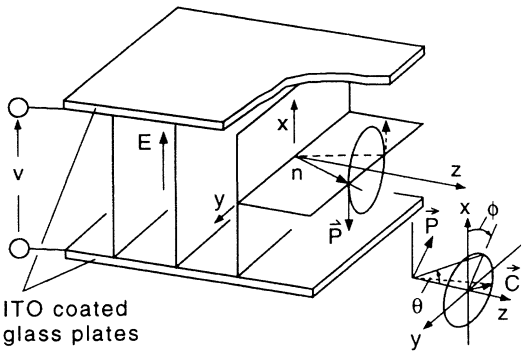

FIG. 1. The bookshelf geometry of a SSFLC cell. The FLC material is between glass plates coated with electrodes of transparent conductor, indium tin oxide (ITO).

is the layer normal and $\hat{\mathbf{y}}$ is parallel to both the layers and the substrates. The angle θ is the cone angle between the molecular long axis (denoted as the director $\hat{\mathbf{n}}$) and the layer normal. For simplicity, the angle θ is assumed to be a constant, solely depending on the temperature of the system. This assumption is most applicable when the temperature of the system is far below the Sm-A^* to Sm-C^* phase-transition temperature T_c [15,7]. The azimuthal angle ϕ is defined as the angle between $\mathbf{P}_s$ and $\hat{\mathbf{x}}$ taking ϕ positive for a right-hand rotation around the negative $\hat{\mathbf{z}}$ axis; $\mathbf{P}_s$ is the ferroelectric polarization which is locally normal to both the $\hat{\mathbf{c}}$ director (the projection of the $\hat{\mathbf{n}}$ director into the smectic planes) and the layer normal $\hat{\mathbf{z}}$. Considering uniform region in the y-z plane, the three-dimensional problem is then reduced into one dimension with the translational velocity $\mathbf{v}=\mathbf{v}(x,t)$ and the azimuth angle $\phi=\phi(x,t)$. We will also neglect the possibility of transportation of material between the smectic layers, i.e., we assume $v_z=0$. Furthermore, as we are studying a sample in the low-velocity regime, we neglect the possibility for the system of developing rolls, i.e., we set $v_x=0$. Thus we are left with two variables $\phi=\phi(x,t)$ and $v=v_y(x,t)$. The above assumptions are consistent with Jakli and Saupe's [7] observations from their electromechanical effect experiments on SSFLC cells.

The previous studies of the dynamics of the SSFLC director field $\hat{\mathbf{n}}(\mathbf{r},t)$ [16–18] have shown that in general in SSFLC's the $\hat{\mathbf{n}}(\mathbf{r})$ is nonuniform and this nonuniformity must be accounted for in any realistic description of $\hat{\mathbf{n}}(\mathbf{r},t)$. The governing equations for the switching dynamics of a SSFLC cell have been derived by us elsewhere [14]. They consist of two coupled equations for the space and time dependence of $\phi(x,t)$ and $v_y(x,t)$, the derivation of which is based on the usual balance of angular and linear momentum, respectively. Thus, in the work presented here we solve the coupled space-time-dependent $\hat{\mathbf{n}}(\mathbf{r},t)$-$\mathbf{v}(\mathbf{r},t)$ fields equations [14], consisting of the usual balances of angular and linear momentum, respectively,

$$\Gamma=L\frac{\partial v}{\partial x}+\eta\frac{\partial\phi}{\partial t}\ , \tag{1}$$

$$\sigma(t)=F\frac{\partial v}{\partial x}+L\frac{\partial\phi}{\partial t}\ , \tag{2}$$

where the coefficients are given as follows:

$$\eta\equiv 2\lambda_5\ , \tag{3}$$

$$L\equiv\lambda_2\cos 2\phi+\lambda_5\ , \tag{4}$$

$$F\equiv\tfrac{1}{2}\mu_0+\tfrac{1}{2}\mu_4+\mu_3\sin^2\phi\cos^2\phi+\lambda_2\cos 2\phi+\tfrac{1}{2}\lambda_5\ , \tag{5}$$

$$\Gamma\equiv H\frac{\partial^2\phi}{\partial x^2}+I\left[\frac{\partial\phi}{\partial x}\right]^2+J\ , \tag{6}$$

$$H\equiv B_1\sin^2\phi+B_2\cos^2\phi\ , \tag{7}$$

$$I\equiv\tfrac{1}{2}(B_1-B_2)\sin 2\phi\ , \tag{8}$$

$$J\equiv -P_sE\sin\phi\ . \tag{9}$$

In developing these equations, P_s is assumed to be small, so that it is reasonable to neglect the dipole-dipole interactions. The modification of the electric field due to the ionic charges [19] is also ignored. Based on the above assumptions, one gets a uniform distribution of electric field $E=V/d$, where V is the applied voltage to the FLC and d is the cell gap. The sign of E is defined as positive when $\mathbf{E}$ is along $\hat{\mathbf{x}}$. The balance of angular momentum equation is given by Eq. (1). The term Γ contains elastic torque terms H and I and the ferroelectric torque (J), while the dielectric torque is neglected in the equations. The L term is the shearing torque, while the η term is the rotational torque. If the coupling between the reorientation of the $\hat{\mathbf{c}}$ director and the mass flow is neglected, Eq. (1) becomes

$$\Gamma=\eta\dot{\phi}\ , \tag{10}$$

where an overdot represents a time derivative. This equation is similar to the switching equation employed by Maclennan, Handschy, and Clark [10]. The balance of linear momentum is given by Eq. (2). In this equation, $\sigma(t)$ is the shear stress exerted on the substrates due to flow $\sigma(t)=\sigma(t)\hat{\mathbf{y}}$. The coefficients λ_i and μ_i are the viscosity coefficients while B_2 and B_1 are the splay and bend elastic constants, respectively, which all are θ dependent except for μ_0 [13,14,20]. The θ dependence of the parameters are expressed in Table I. As an approximation we take $\bar{P}_s$, $\bar{B}_i$, $\bar{\lambda}_i$, and $\bar{\mu}_i$ to be temperature independent, with the principal temperature dependence of the equations hidden in their θ dependence. We expect that the bar viscosities, for instance, $\bar{\mu}_0$, the isotropic part of the viscosities, will also have some temperature dependence. The θ-dependent viscosities in Table I are those coming from the reorientation of an $\hat{\mathbf{n}}$ ignoring the biaxiality of smectic-C phase. Additional terms arising from

TABLE I. Scaling of parameters and their values.

Scalings	Values
$\lambda_2=\bar{\lambda}_2\sin^2\theta$	$\bar{\lambda}_2=-11$ sec erg/cm^3
$\lambda_5=\bar{\lambda}_5\sin^2\theta$	$\bar{\lambda}_5=7.5$ sec erg/cm^3
$\mu_0=\bar{\mu}_0$	$\bar{\mu}_0=1.875$ sec erg/cm^3
$\lambda_3=\bar{\lambda}_3\sin^4\theta$	$\bar{\mu}_3=0.0$ sec erg/cm^3
$\lambda_4=\bar{\lambda}_4\sin^2\theta$	$\bar{\mu}_4=9.6$ sec erg/cm^3
$B_i=\bar{B}_i\sin^2\theta$	$\bar{B}_1=\bar{B}_2=7.1$ dyne
$P_s=\bar{P}_s\sin\theta$	$\bar{P}_s=29.0$ nC/cm^3

the biaxiality are expected to be small for θ's in the typical operating range, so they have not been included here.

From Eqs. (1) and (2), one gets

$$\frac{\partial v}{\partial x}=\frac{\eta\sigma-L\Gamma}{\eta F-L^2}=\frac{\frac{\sigma}{F}-A\frac{\Gamma}{L}}{1-A}\ , \tag{11}$$

$$\dot{\phi}=\frac{F\Gamma-\sigma L}{\eta F-L^2}=\frac{\frac{\Gamma}{\eta}-A\frac{\sigma}{L}}{1-A}\ , \tag{12}$$

where

$$A(\phi,\theta)\equiv\frac{L^2}{\eta F}=\frac{(\lambda_2\cos2\phi+\lambda_5)^2}{\lambda_5(\mu_0+\mu_4+\frac{1}{2}\mu_3\sin^2 2\phi+\lambda_5+2\lambda_2\cos2\phi)}\ . \tag{13}$$

This quantity is a function which characterizes whether the flow effect is weak or strong, introduced in studying the dynamics of an electrically induced Fréedericksz transition in SSFLC cells [21] in a way similar to that used in nematic liquid crystals by Brochard and coworkers [22,23]. One should note that the function A depends on both ϕ and θ, thus adopting different values in different parts of the cell. By adopting the usual nonslip conditions at the interfaces, i.e., $v(0,t)=0$ and $v(d,t)=0$, Eq. (11) can be integrated to read

$$\sigma(t)=\frac{\int_0^d\frac{L\Gamma}{\eta F-L^2}dx}{\int_0^d\frac{\eta}{\eta F-L^2}dx}=\frac{\int_0^d\frac{A\frac{\Gamma}{L^2}}{1-A}dx}{\int_0^d\frac{1}{F(1-A)}dx}\ . \tag{14}$$

From Eqs. (11), (12), and (14) it is clear that for $A\to0$, both σ and $\partial v/\partial x$ approach zero. In this case Eqs. (12) and (10) become identical and, as also can be seen from Eq. (1), backflow effects will be absent in the system. As will be shown in the next section, when $A\to1$ backflow effects become more pronounced. We also see that for $A=1$, Eq. (14) develops singularities. The calculations presented in this work are only for $0<A<1$, a limit resulting from the requirement of positive dissipation of energy [21].

Plugging Eq. (14) into Eq. (12), one gets a highly nonlinear diffusion type of integral-differential equation. To solve this equation, a general scheme of the Crank-Nichlson method has been used. In each time step, an iteration is employed to solve the ordinary integral-differential equation. In each time step, the calculation of $\sigma(t)$ begins with the ϕ from the previous time step. The σ is used in Eq. (12) to get a new ϕ, which is used in Eq. (14) to get σ. This procedure goes on until a convergence criterion is satisfied. Strong anchoring is assumed in the calculation, i.e., fixed boundary conditions for ϕ are used, $\phi(0,t)=\phi_0$ and $\phi(d,t)=\phi_d$. Also, for simplicity, $\bar{B}_2$ is taken to be equal to $\bar{B}_1$.

III. NUMERICAL RESULTS

In order to solve Eqs. (1) and (2) numerically, some numbers must be assigned to all the material parameters entering those equations. Today no experimental information is available for most of these parameters. However, based on thermodynamic arguments, Carlsson, Leslie, and Clark [20] have suggested a set of model parameters which are based on nematic values consistent with all presently known inequalities these parameters must fulfill. We have used a slightly modified set of parameters and chosen the values given in Table I. In order to study the different regions for which backflow effects are pronounced ($A\to1$) or not ($A\to0$), we have simply changed the tilt angle θ at the system (cf. Fig. 2).

The natural time scale for Eq. (10) is $\tau=\eta/P_sE$, while the natural length scale is defined as $\xi=\sqrt{B_1/P_sE}$. The critical field $E_c\equiv B_1\pi^2/P_sd^2$, for which the Fréedericksz transition is induced, has been calculated in Ref. [21]. Throughout this paper, we use reduced field which is defined as $\varepsilon=E/E_c$.

A. Orientation dynamics in the bookshelf geometry with $\phi_0=0$ and $\phi_d=\pi$ (the bend-splay cell)

First we consider the problem of a bookshelf cell with $\phi_0=0$ and $\phi_d=\pi$. The cell geometry is shown in Fig. 1. The boundary conditions $\phi_0=0$ and $\phi_d=\pi$ mean that at the bottom and the top substrate the polarization is pointing up and down, respectively. At zero applied electric field, the initial state is a combined bend-splay deformation of the $\hat{c}$ director. When a positive electric field is turned on the molecules start to switch, except at the top glass since there the strong boundary condition $\phi=\pi$ is enforced. Figure 3 shows the switching processes for three different applied fields, with case (a) for $\varepsilon=3.6475$ implying $d/\xi=6$, (b) for $\varepsilon=100$ and (c) for $\varepsilon=364.75$.

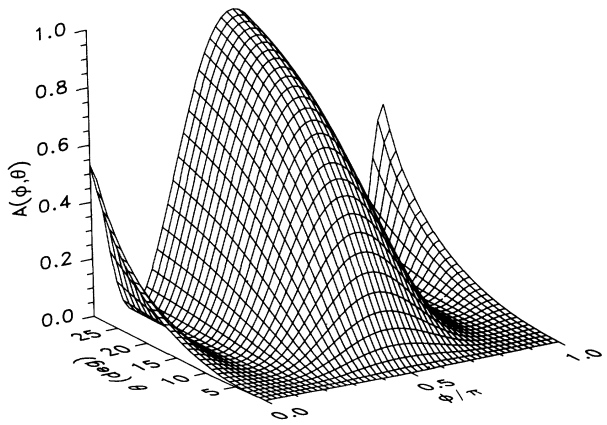

FIG. 2. The control parameter $A(\phi,\theta)$ calculated for the set of viscosity coefficients given in Table I. For a small value of A, backflow effects are weak, while they become very pronounced as A approaches unity.

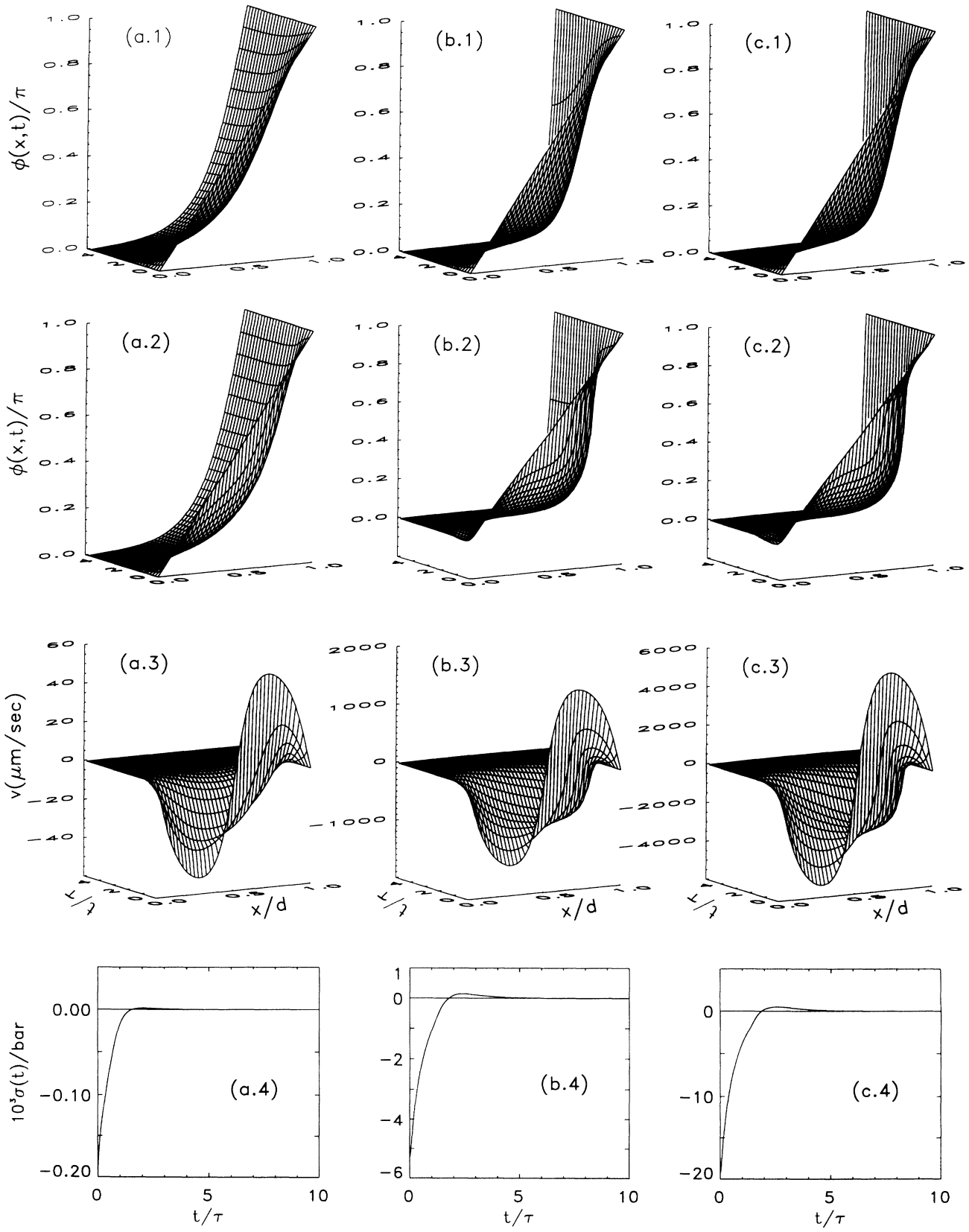

FIG. 3. Response of a SSFLC cell with boundary conditions $\phi=0$ and π on the two bounding plates, respectively. The electric field used in the calculations is $\varepsilon=3.6475$, 100, and 364.75 for columns (a), (b), and (c), respectively. The upper row depicts the c-director profile $\phi(x,t)$ calculated when backflow effects are neglected, while for the second row backflow effects have been included in the calculations. Row 3 shows the velocity profile $v(x,t)$ which develops during the switching and row 4 shows the shear stress $\sigma(t)$ excerted on the substrates due to the backflow.

The cone angle θ is taken as 22.5° in all the three columns. The switching processes in the cases when the backflow is neglected are shown in row 1 of Fig. 3. Here a two-dimensional plot of ϕ as a function of x/d and t/τ is depicted. The switching dynamics when backflow effects are taken into account is shown in row 2 of Fig. 3, while the corresponding flow profiles are plotted in row 3 of the figure. Row 4 of Fig. 3 depicts the time dependence of the shear stress $\sigma(t)$ corresponding to the calculations for which backflow effects have been taken into account. When $\varepsilon=3.6475$, the differences are small between $\phi(x,t)$ in Fig. 3(a.2) and $\phi(x,t)$ in Fig. 3(a.1), calculated with and without taking backflow into account, except that the switching process becomes slightly faster when backflow is present. This can be qualitatively understood as follows: Starting with states in which ϕ_x is a constant, at $t=0^+$, the molecules at the middle plane, e.g., at $x=\frac{1}{2}d$, which experience the largest electric-field torque relative to those at the other positions, are not flowing due to symmetry; in the middle plane, the $\hat{c}$ director is at the vertical position and rotates counterclockwise (looking from the $+\hat{z}$ direction into the $-\hat{z}$ direction), which, acting like a paddle wheel, pushes the molecules above the middle plane to flow to the left (thus $v>0$) and the molecules below the middle plane to flow to the right (thus $v<0$), and this effect in turn helps the switching at the middle plane to be faster. Since the velocities at the interfaces are set to be zero, the net result of velocity at $t=0^+$ is like a negative sine function. As time goes on, the system reaches the steady state. Thus the velocity profile $v(x,t)$ and the shear stress both go to zero, as shown in Figs. 3(a.3) and 3(a.4), respectively. When the field strength is increased, as for the cases depicted in Figs. 3(b) and 3(c), the backflow effects become more pronounced. The increase in the magnitude of flow and shear stress is almost proportional to the increase of the field strength, as seen from Figs. 3(b) and 3(c). This result can be understood from Eqs. (11) and (14), since, at $t=0, \Gamma=J$, which is linear in the electric field. One notices from Figs. 3(b.2) and 3(c.2) that the backflow effect forces the molecules, near the bottom substrate where the electric-field torque is weak relative to the shear flow torque, to the "wrong" direction before the system reaches its final state.

In the above we have considered the influence of backflow effects under different applied fields. Now we consider how these effects depend on the value of the function A under the same applied electric field ε. The variation of the A values can be achieved by either changing the cone angle θ or replacing the values of the viscosity coefficients. Calculations have been carried out for different A's by changing either θ or μ_i's. All the calculations reach the same conclusion that, as indicated from Eqs. (11), (12), and (14), the larger the A value is, the stronger will the flow effect be. For the above cell, at $t<0$, an up field $\varepsilon=364.75$, which makes $d/\xi=60$ applied to the cell. At $t=0$, a down field with same magnitude is applied to the cell. The results of the simulations are shown in Fig. 4, where column (a) is for $\theta=1.0°$, (b) is for 14.0°, and (c) is for 22.5°. In the case when a strong applied positive field is applied, the polarization aligns up with the field everywhere except near the top glass where there is a π kink (ϕ varies from 0 to π in a very thin layer). When the sign of the applied electric field is changed, most of the polarization will be in an unstable equilibrium except at the π kink, e.g., the torque due to $\mathbf{P}_s\times\mathbf{E}$ is zero everywhere except at the kink. The kink, or soliton, will then propagate across the cell in a time $\Delta t\approx\tau(d/\xi)$, roughly 60 times longer than it takes to equilibrate from the relaxed (bend-splay) state. This increase in switching time is a result of the configuration upon field reversal having nearly all the dipoles in unstable equilibrium. The dipoles which are at the unstable equilibrium state will stay there until the soliton wave reaches, assuming there is no other force to reorient them earlier. This results in a solitary wave traveling across the cell as shown in Fig. 4(a.1), for which the calculation has been performed by neglecting backflow effects. This is the same result as reported in Ref. [10]. When the backflow effects are taken into account, the flow helps to tilt the dipoles away from their equilibrium state, so that the molecules can experience the electric-field torque even before the solitary wave reaches. This situation is shown in Fig. 4(a.2). The flow profile is shown in Fig. 4(a.3) and the shear stress of this case is shown in Fig. 4(a.4). In case (a), the average of $A(\phi)$ over ϕ is about 0.0007, i.e., $\langle A\rangle=0.0007$. Even for such a small value of $\langle A\rangle$, the solitary wave is wiped out by a uniform reorientation before crossing the middle of the cell. This occurs because at the unstable equilibrium state the flow-induced torques reorient them to experience the electric torque before the solitary wave reaches. Thus the influence of backflow is clear when comparing Figs. 4(a.1) and 4(a.2). When the cone angle is increased, the value of function A is also increased. Figure 4(b) shows the case for $\theta=14°$, in which the molecules near the top glass are overrotating as shown in Fig. 4(b.2). When the cone angle is increased further, besides the overrotating effect near the top glass, the molecules near the bottom are rotated to the "wrong" direction before turning to positive π direction. When the molecules are uniformly at the $\phi=0$ position or the $\phi=\pi$ position, the Γ's are equal to zero, thus the only torque is from the shear flow as seen in Eq. (12). So the negative shear stresses at $t=3\tau$ and 7τ as shown in Fig. 4(c.4) are the cause of the wrong rotations in Fig. 4(c.2). In the case when A is even larger, a 2π wall appears near $x=0$. This calculation is, however, not shown here, but a similar creation of a 2π wall is depicted in Fig. 5(c.2). By comparing the cases (a), (b), and (c), we see that the shear stress in case (b) (where $\langle A\rangle=0.10$) is about two orders of magnitude larger than that in case (a), while the stress in case (c) (where $\langle A\rangle=0.3$) is about double that in case (b). One notices that the complete switching in Fig. 4(a.2) takes about 11τ while the switching in Fig. 4(c.2) takes only about 5τ. From the figure it is clear that the smaller the value of $\langle A\rangle$, the smaller the difference between the solution to the governing equations in the cases when backflow effects are taken into account or not. Comparing rows 1 and 2 of Fig. 4, we see that the switching time in the calculations when backflow effects are taken into account are generally faster than for the case when backflow effects are neglected.

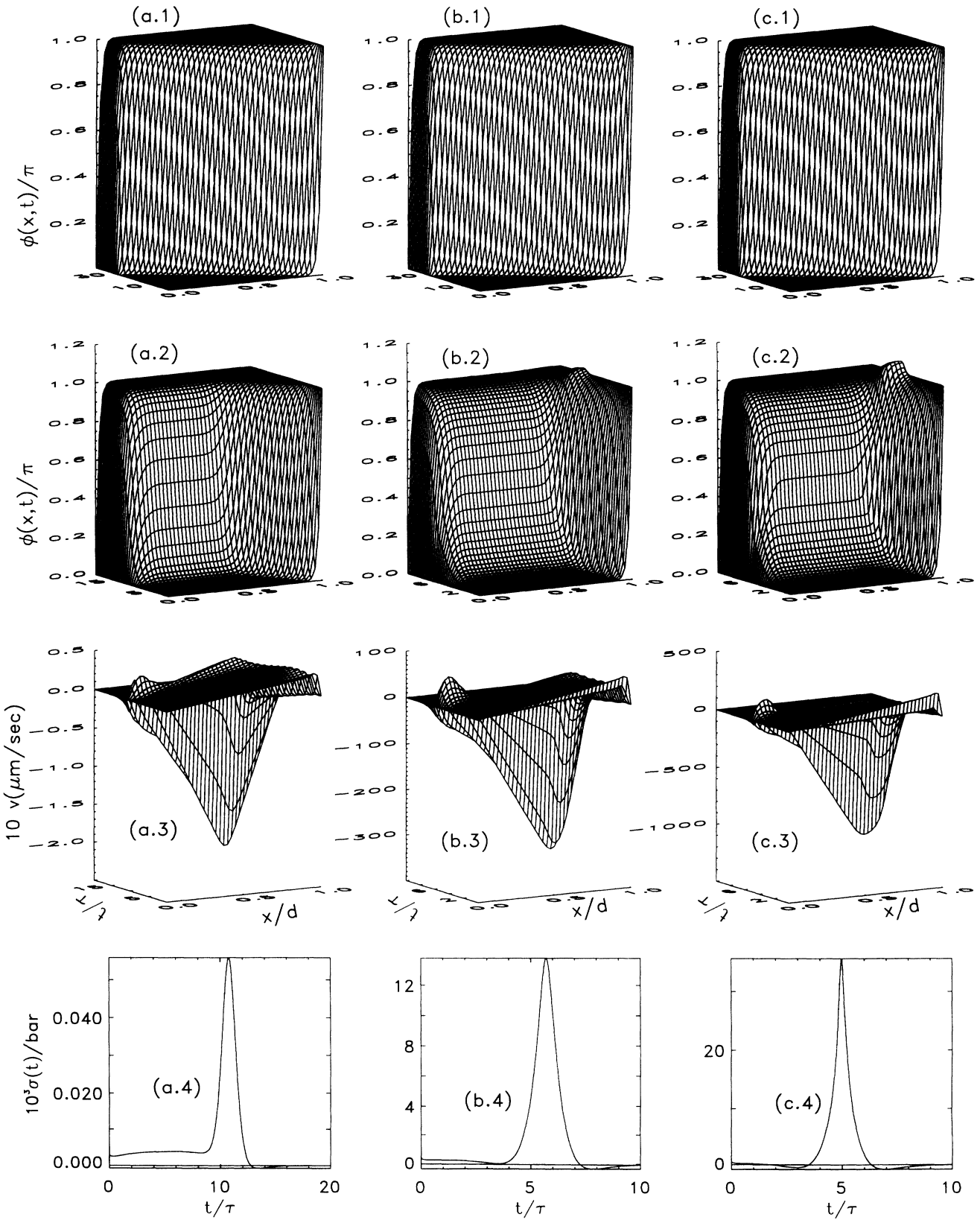

FIG. 4. Response of a SSFLC cell with boundary conditions $\phi=0$ and π on the two bounding plates, respectively. The applied electric field is changed instantaneously at $t=0$ from $\varepsilon=364.75$ to -364.75 and the average value of the control parameter A used in the calculations in $\langle A \rangle=0.0007$, 0.1, and 0.3 for columns (a), (b), and (c), respectively. The arrangement of rows is the same as in Fig. 3.

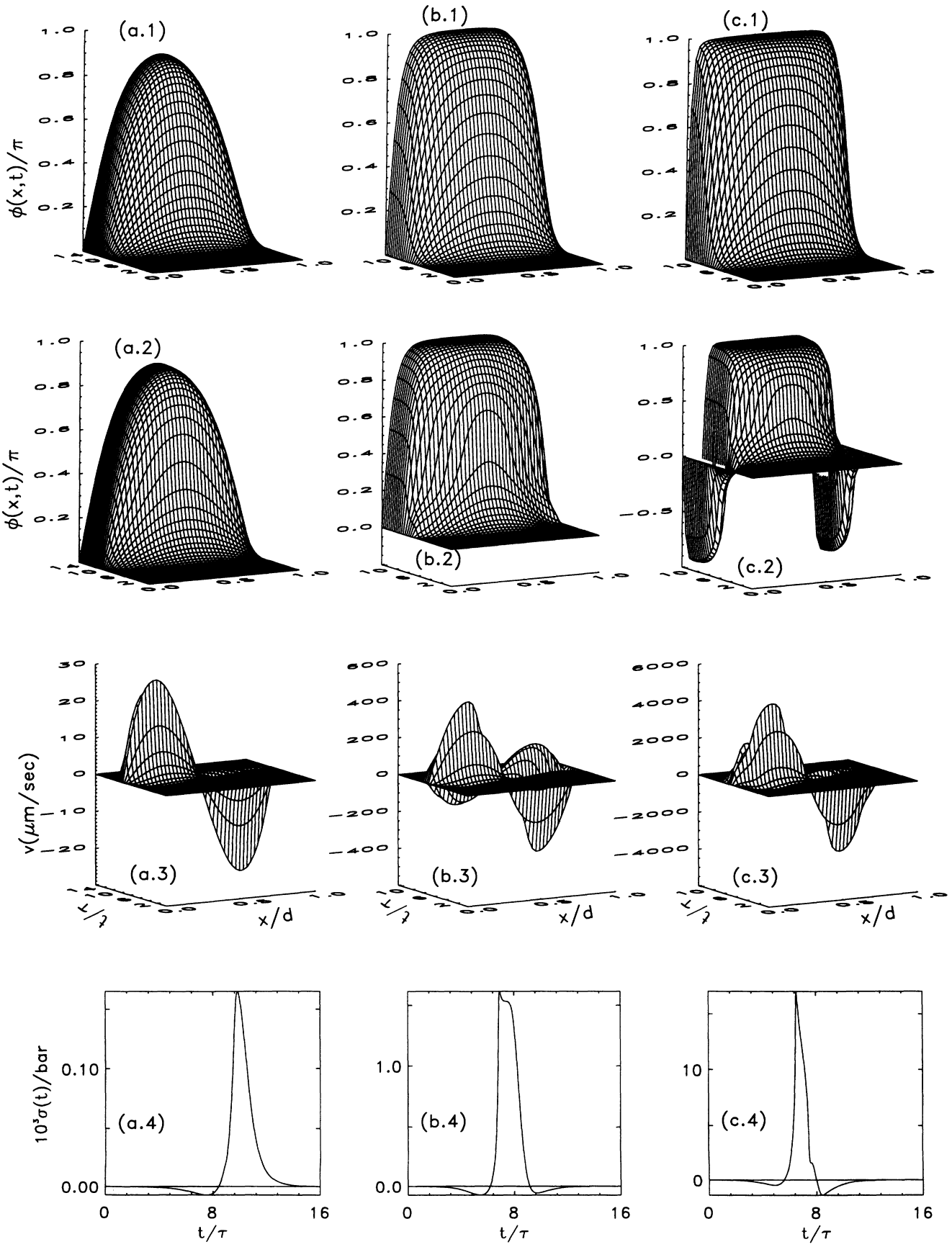

FIG. 5. Dynamics of a Fréedericksz transition. The electric field used in the calculations is $\varepsilon = -3.647$, -100, and -364.75 for columns (a), (b), and (c) respectively. The arrangement of rows is the same as in Fig. 3.

B. Orientation dynamics in the bookshelf geometry with $\phi_0=0$ and $\phi_d=0$ (Fréedericksz transition in a SSFLC cell)

Next we will consider the problem of a bookshelf cell with $\phi_0=0$ and $\phi_d=0$, i.e., the Fréedericksz transition in a SSFLC cell. The analytical solution of this problem in a small ϕ approximation is published elsewhere [21]. Here the general numerical solutions of this problem is presented.

First we investigate the influence of backflow under different applied fields. The equilibrium state for zero field of this cell has all the dipoles uniformly pointing upwards. Applying a downward field to the cell, the switching dynamics will develop as depicted in Fig. 5. In this figure, columns (a), (b), and (c) correspond to $\varepsilon=-3.647$, -100, and -364.75, respectively. The switching profiles in the case when backflow is neglected are shown in row 1 of the figure. We see that the switching times are about 10τ in all three cases, since the field is included in the expression of τ already. The different final states of row 1 of Fig. 5 are due to the different applied fields. The switching profiles when backflow effects are taken into account are much different and are shown in row 2 of Fig. 5. Due to the small electric field in case (a), there is almost no differences between (a.1) and (a.2), except that the switching in (a.2) is somewhat faster than that in (a.1). When the field is increased, the differences between c-director profiles calculated by neglecting backflow effects and taking into account increase. In case (b), where $\varepsilon=-100$, the switching time, for the case when backflow effects are taken into account, (b.2), is roughly two-thirds of that being calculated when backflow effects are neglected, (b.1). Due to the strong flow effect, the molecules near the boundaries, where the azimuthal angle ϕ is closer to zero than at the middle of the cell, rotates to the wrong direction before the elastic force pulls them back. With an even stronger field, as is the case in Fig. 5(c), the ferroelectric torque dominates over the elastic torque and the final configuration exhibits two 2π walls close to the substrates. As in Sec. III A, we have demonstrated that the larger the applied electric field is (the faster the switching is), the more pronounced will the backflow effects be.

Now we consider how the backflow effects are affected by changing the values of the function A. As in Sec. IV A, we vary A by varying the cone angle θ. The results are shown in Fig. 6, where columns (a), (b), and (c) are calculated for $\theta=14°$ ($\langle A\rangle=0.1$), $\theta=20°$ ($\langle A\rangle=0.18$), and $\theta=22.5°$ ($\langle A\rangle=0.3$), respectively. The applied field used in the calculation of Fig. 6 is $\varepsilon=-364.75$. Thus column (c) of Fig. 6 is the same as column (c) of Fig. 5. When θ is reduced, the average value $\langle A\rangle$ reduces correspondingly and we notice that the backflow effects become less pronounced. This observation is in accordance with the results of the calculations presented in Fig. 4.

Next we consider how the molecules relax to their equilibrium states when the field is turned off. Still we consider the cell with boundary conditions $\phi_0=\phi_d=0$. The isotropic part of viscosity μ_0 is reduced to 1.0 so that the value of A can be larger, thus with stronger backflow effect. The cone angle in this calculation is once again taken to be 22.5°. In order to avoid the formation of 2π walls due to the application of the strong electric field, the field is gradually increased from $\varepsilon=0$ to -364.75. After the cell is exposed to the large negative field for a long time, the azimuthal angle $\phi(x,t)$ reaches its equilibrium state, which is the initial state for the problem considered below. Turning the field off, the elastic torque will bring the molecules back to equilibrium state $\phi=0$. Since we study the relaxation of the system in the zero applied electric field, the characteristic time scale of the system is chosen to be $\tau_0=\eta d^2/K_1$. If backflow effects are neglected, the system relaxes back to the state $\phi=0$ solely under the influence of the elastic torque. When backflow effects are taken into account in the calculations, the character of the switching is changed. The backflow effects cause ϕ in the middle of the cell to initially increase before decreasing to zero. In Fig. 7 $\phi(d/2,t)$ is depicted in the middle of the cell calculated when backflow effects are taken into account (solid line) and when backflow effects are neglected (dashed line). Assume that under crossed polarizers we define the up state as the bright state and the down state as the dark state. According to Fig. 7 the transmittance of the cell will first decrease, then increase slightly due to the backflow in the cell, before finally relaxing to zero. This effect is similar to that observed as a result of backflow in the twisted nematic cells [3,4].

IV. CONCLUSIONS

By employing the recently developed elastic-hydrodynamic theory of the Sm-C^* phase [8], in this work we have investigated the role of backflow effects in the switching dynamics of a SSFLC cell for a few different cell geometries. Although, for a complete description of the system twenty viscosity coefficients and nine elastic constants are needed, for the switching analyzed in this work only five viscosities and two elastic constants enter the governing equations (1)–(10). These material parameters must fulfill [20] certain inequalities as well as the scaling relations discussed in Sec. II. By employing this scaling we introduced the constants $\bar{\lambda}_2$, $\bar{\lambda}_5$, $\bar{\mu}_0$, $\bar{\mu}_3$, $\bar{\mu}_4$, $\bar{B}_1$, and $\bar{B}_3$ (cf. Table I), the temperature dependence of which is neglected as an approximation. In this way the temperature dependence of our results implicitly enters through the θ dependence of the governing equations.

From a previous analytical study of the governing equations [21], we have been able to identify the control parameter $A(\phi,\theta)$ [cf. Eq. (14)], determining whether or not backflow effects will be of importance when studying a specific problem. It can be proven [21] that $A(\phi,\theta)$ is positive definite and by stability reasons we restrict the study in this work to cover only the case $A(\phi,\theta)<1$. We believe that this inequality should be the consequence of thermodynamic stability of the system, but we cannot presently derive a formal proof for this. Whenever A is small, backflow effects are negligible, while they become important as A approaches unity. This is clearly demonstrated by the numerical solutions to the governing equations presented in Figs. 4 and 6.

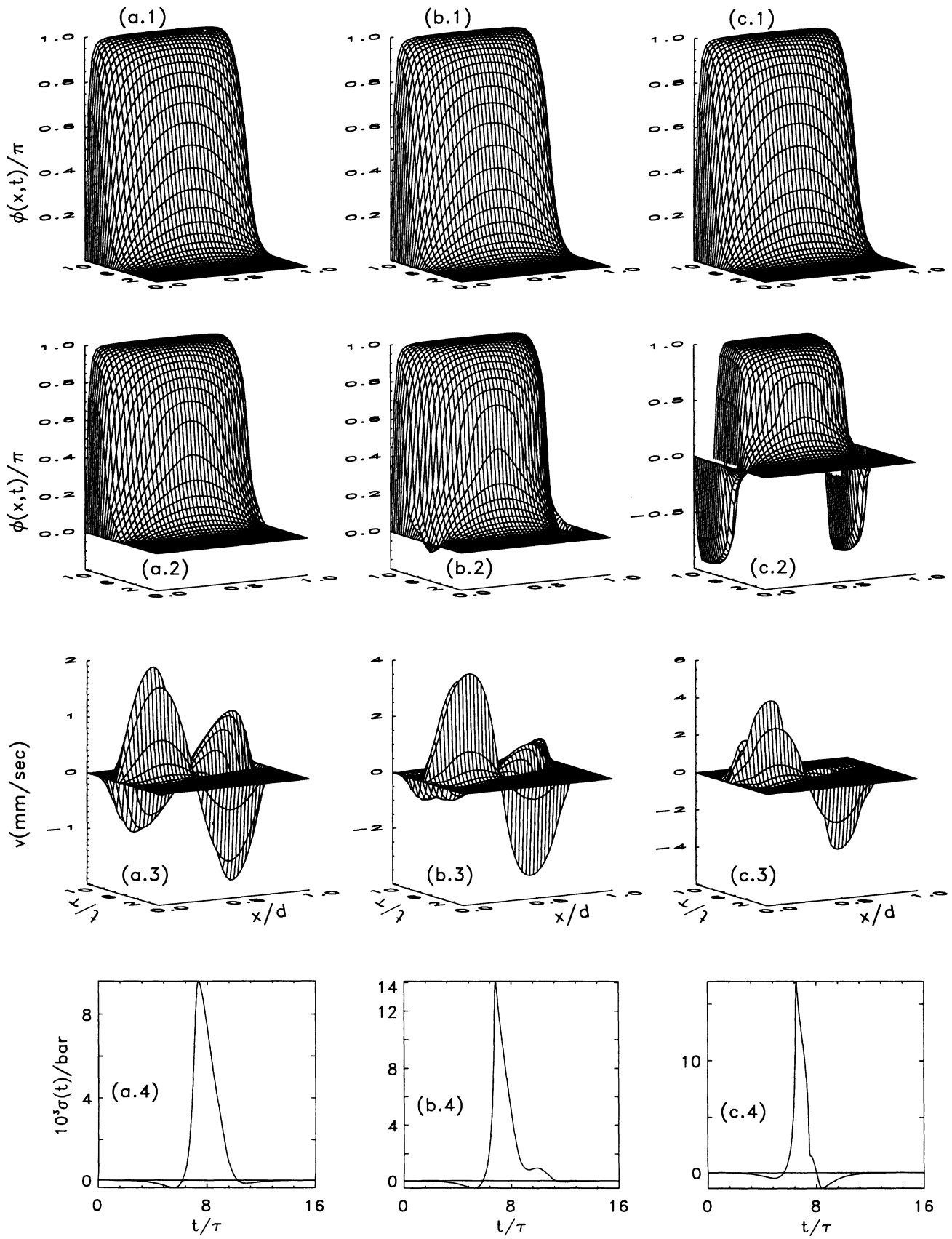

FIG. 6. Dynamics of a Fréedericksz transition. The electric field is $\varepsilon = -364.75$ and the average value of the control parameter A used in the calculations is $\langle A \rangle = 0.1$, 0.18, and 0.3 for columns (a), (b), and (c), respectively. The arrangement of rows is the same as in Fig. 3.

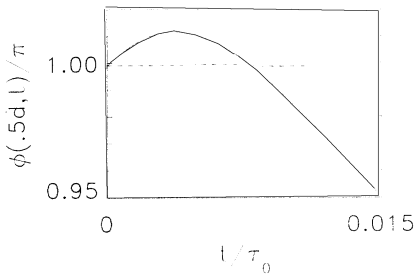

FIG. 7. Relaxation of a Fréedericksz cell to its equilibrium state. The azimuthal angle $\phi(d/2,t)$ in the middle of the cell is shown in the cases when backflow effects are taken into account (solid line) and when backflow effects are neglected (dashed line).

The main results of this paper are presented in Figs. 3–7. In Figs. 3–6 we compare the time evolution of the $\hat{c}$-director profile $\phi(x,t)$ when the governing equations of the system are solved by either neglecting backflow effects (row 1) or by including these into the calculations (row 2). Two different cell geometries are studied: the bend-splay cell (Figs. 3 and 4) and a Fréedericksz transition (Figs. 5 and 6). By comparing the two upper rows of the figures we notice that the backflow effects not only change the cell behavior quantitatively, but also in some cases qualitatively. One example of this is the driving of a solitary wave through the cell depicted in Fig. 4. As is shown in the figure, due to backflow effects the molecules start rotating before the solitary wave reaches their position, thus wiping out the soliton, also speeding up the switching time of the cell. Another interesting qualitative change in the switching behavior of the cell which backflow effects can induce is the creation of 2π walls in the system as depicted in Figs. 5(c) and 6(c). When the backflow effects are pronounced, the switching close to the substrates starts in the "wrong" direction. If the electric field is large enough, the ferroelectric torque dominates over the elastic torque and the final configuration of the cell exhibits two 2π walls close to the bounding plates. Thus a large applied electric field is not necessarily the best for the cell performance if one wants to achieve a homogeneous final state. The 2π walls can be avoided by increasing E to its final E_f sufficiently slowly, i.e., over a period $\sim 10\tau_f = 10\eta/P_s E_f$.

In conclusion, in this paper we have shown that backflow effects should be expected to influence the switching behavior of a SSFLC cell in most cases. We have been able to identify the control parameter $A(\phi,\theta)$ [Eq. (14)], the value of which determines whether backflow effects are of importance or not. Since today very little information of the values of the viscosity coefficients of the Sm-C^* phase exists, we cannot make any statements regarding experimental values of $A(\phi,\theta)$.

ACKNOWLEDGMENTS

This work was supported in part by ARO Contract No. DAAHO4-93-G-0164 and NSF Engineering Research Optoelectronic Computing Systems Center Grant No. CDR 8622236.

[1] J. L. Ericksen, Trans. Soc. Rheol. **5**, 23 (1961).
[2] F. M. Leslie, Arch. Ration. Mech. Anal. **28**, 268 (1968).
[3] C. J. van Doorn, J. Appl. Phys. **46**, 3738 (1975).
[4] D. W. Berremann, J. Appl. Phys. **46**, 3746 (1975).
[5] N. A. Clark and S. T. Lagerwall, Appl. Phys. Lett. **36**, 889 (1980).
[6] A. Jakli and A. Saupe, Liq. Cryst. **9**, 519 (1991).
[7] A. Jakli and A. Saupe (unpublished).
[8] F. M. Leslie, I. W. Stewart, and M. Nakagawa, Mol. Cryst. Liq. Cryst. **198**, 443 (1991).
[9] F. M. Leslie, Liq. Cryst. **14**, 121 (1993).
[10] J. E. Maclennan, M. A. Handschy, and N. A. Clark, Phys. Rev. A **34**, 3554 (1986); J. E. Maclennan, N. A. Clark, and M. A. Handschy, in *Solitons in Liquid Crystals,* edited by L. Lam and J. Prost (Springer-Verlag, Berlin, 1991).
[11] N. A. Clark and S. T. Lagerwall, in *Ferroelectric Liquid Crystals: Principles, Properties and Applications,* edited by J. W. Goodby *et al.* (Gordon and Breach, New York, 1991).
[12] N. Hiji, Y. Ouchi, H. Takezoe, and A. Fukuda, Jpn. J. Appl. Phys. **27**, 11 (1988).
[13] T. Carlsson, I. W. Stewart, and F. M. Leslie, Liq. Cryst. **9**, 661 (1991).
[14] Z. Zou, N. A. Clark, and T. Carlsson (unpublished).
[15] T. Carlsson and I. Dahl, Mol. Cryst. Liq. Cryst. **95**, 373 (1983).
[16] J. E. Maclennan, N. A. Clark, M. A. Handschy, and M. R. Meadows, Liq. Cryst. **7**, 753 (1990).
[17] P. C. Willis, N. A. Clark, and J. Z. Xue (unpublished).
[18] Z. Zhuang, N. A. Clark, and J. E. Maclennan, Liq. Cryst. **10**, 409 (1991).
[19] Z. Zou, N. A. Clark, and M. A. Handschy, Ferroelectrics **121**, 147 (1991).
[20] T. Carlsson, F. M. Leslie, and N. A. Clark (unpublished).
[21] T. Carlsson, N. A. Clark, and Z. Zou, Liq. Cryst. **15**, 461 (1993).
[22] F. Brochard, P. Pieranski, and E. Guyon, Phys. Rev. Lett. **28**, 1681 (1972).
[23] P. Pieranski, F. Brochard, and E. Guyon, J. Phys. (Paris) **34**, 35 (1973).

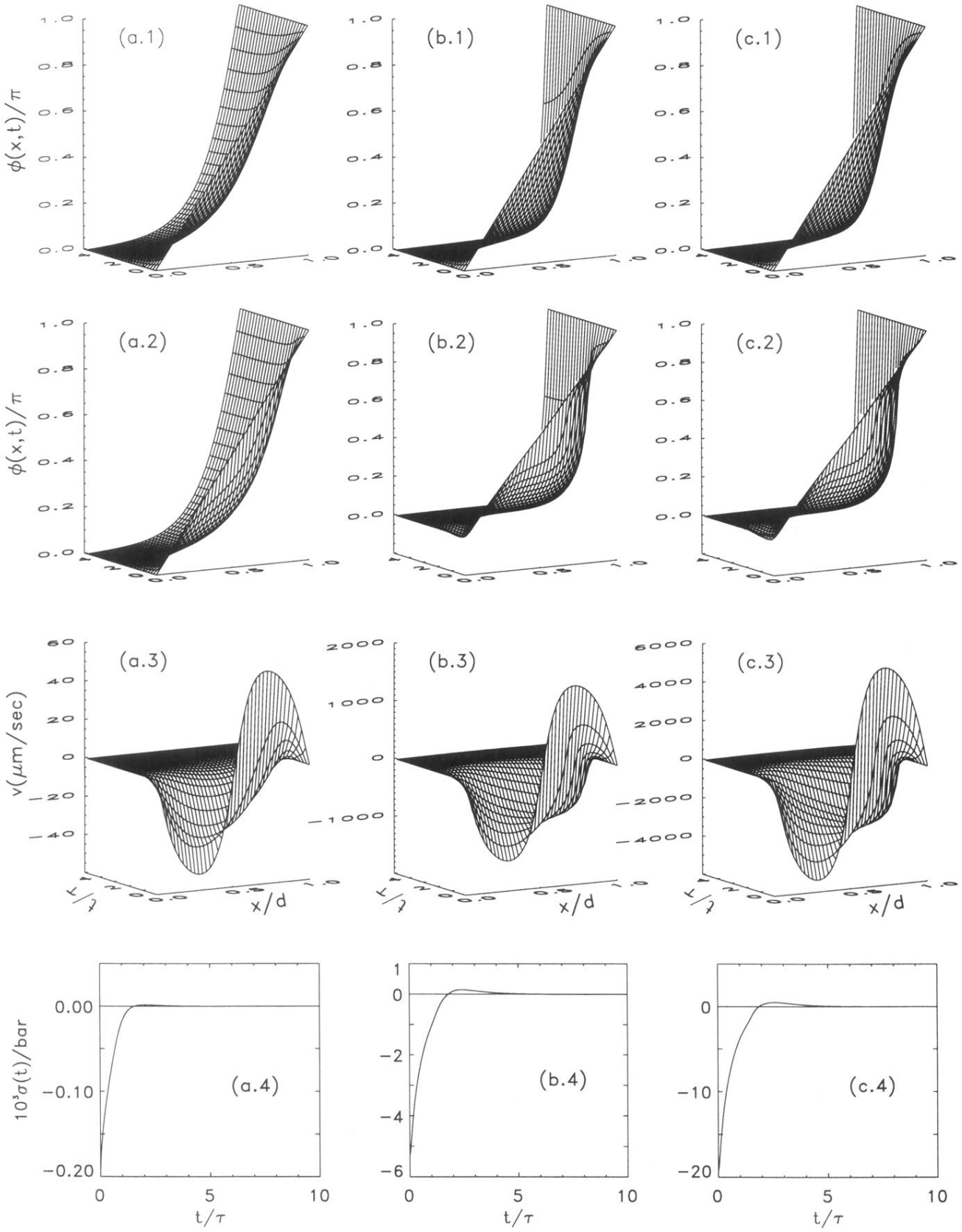

FIG. 3. Response of a SSFLC cell with boundary conditions $\phi=0$ and π on the two bounding plates, respectively. The electric field used in the calculations is $\varepsilon=3.6475$, 100, and 364.75 for columns (a), (b), and (c), respectively. The upper row depicts the c-director profile $\phi(x,t)$ calculated when backflow effects are neglected, while for the second row backflow effects have been included in the calculations. Row 3 shows the velocity profile $v(x,t)$ which develops during the switching and row 4 shows the shear stress $\sigma(t)$ excerted on the substrates due to the backflow.

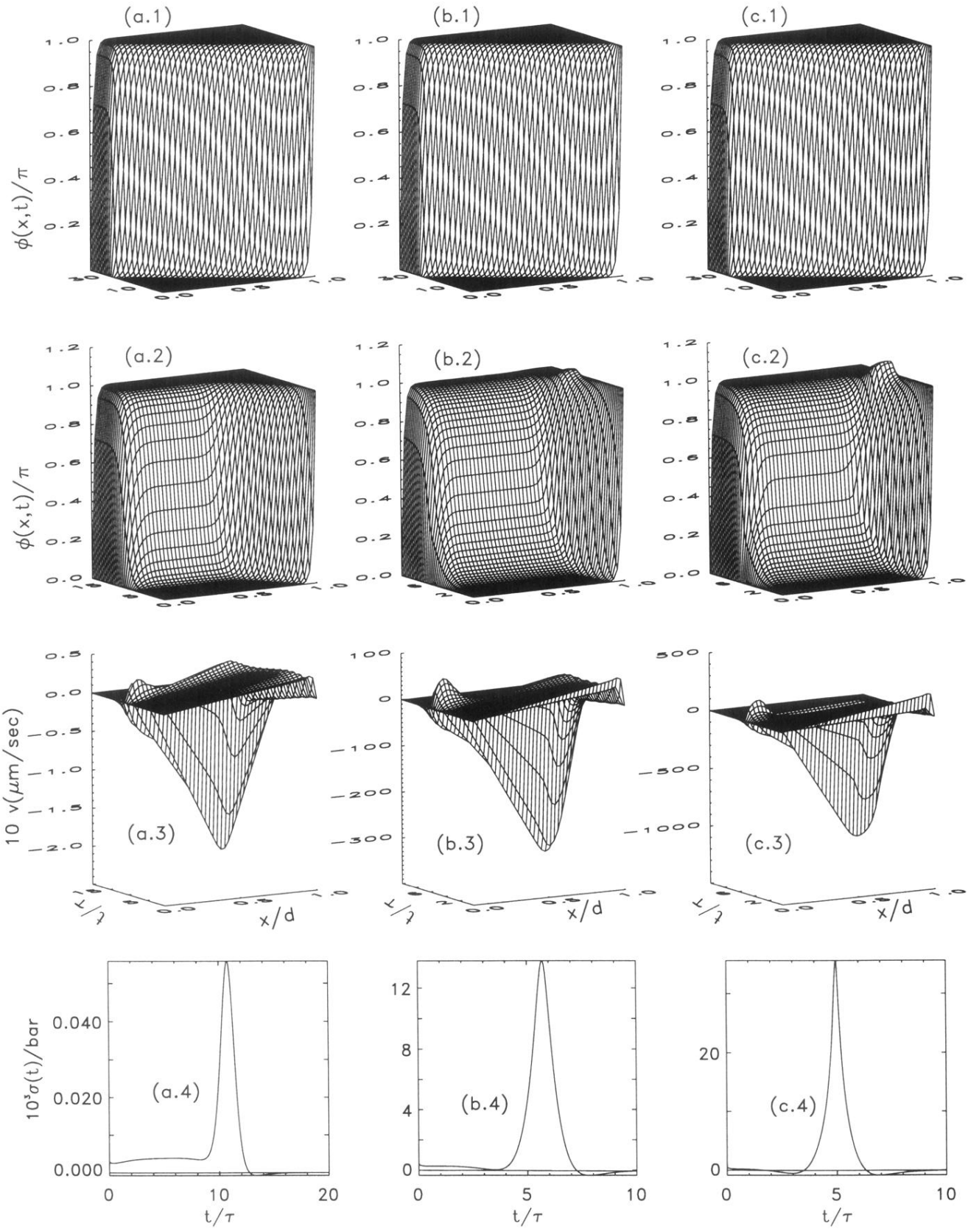

FIG. 4. Response of a SSFLC cell with boundary conditions $\phi=0$ and π on the two bounding plates, respectively. The applied electric field is changed instantaneously at $t=0$ from $\varepsilon=364.75$ to -364.75 and the average value of the control parameter A used in the calculations in $\langle A \rangle=0.0007$, 0.1, and 0.3 for columns (a), (b), and (c), respectively. The arrangement of rows is the same as in Fig. 3.

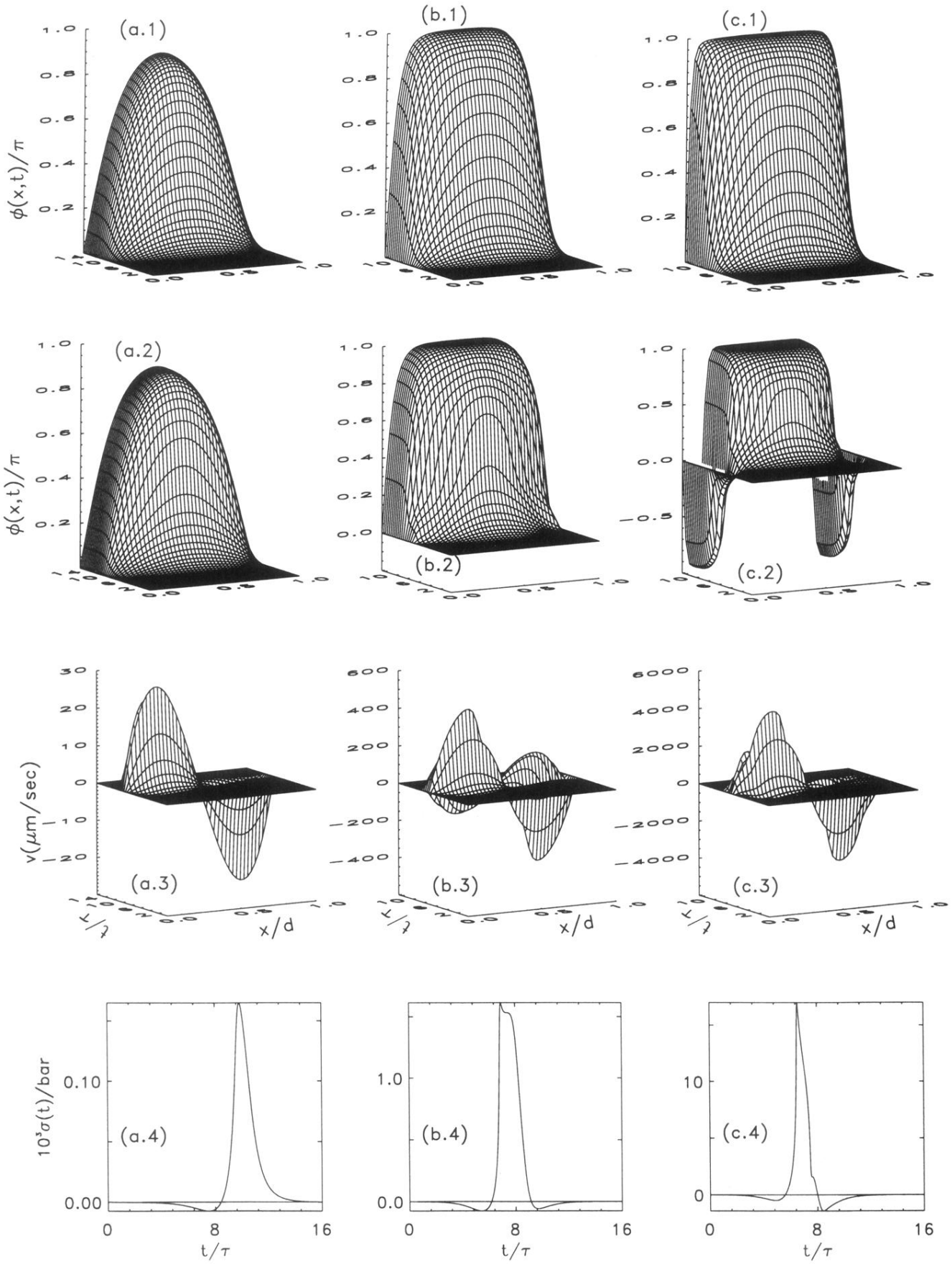

FIG. 5. Dynamics of a Fréedericksz transition. The electric field used in the calculations is $\varepsilon = -3.647$, -100, and -364.75 for columns (a), (b), and (c) respectively. The arrangement of rows is the same as in Fig. 3.

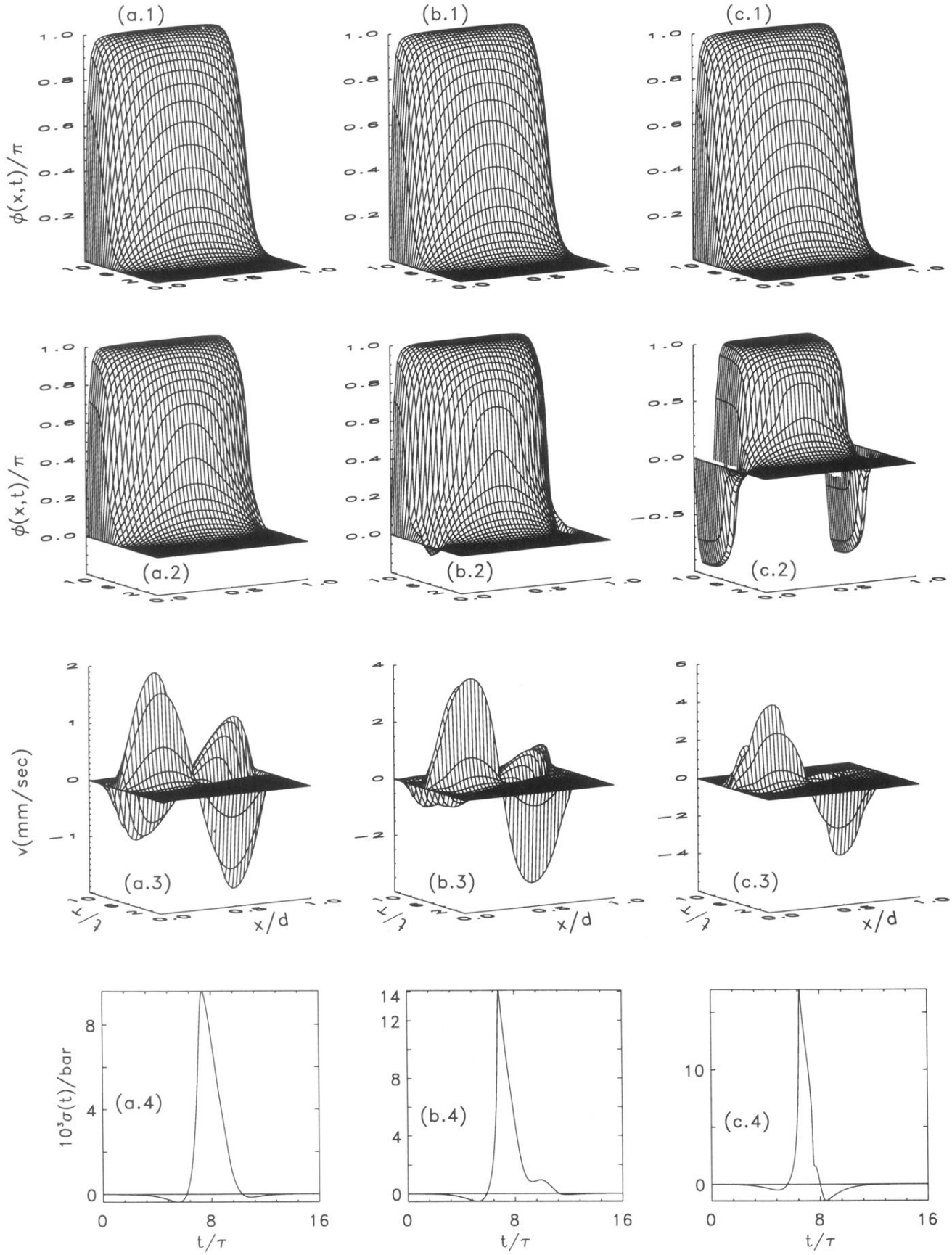

FIG. 6. Dynamics of a Fréedericksz transition. The electric field is $\varepsilon = -364.75$ and the average value of the control parameter A used in the calculations is $\langle A \rangle = 0.1$, 0.18, and 0.3 for columns (a), (b), and (c), respectively. The arrangement of rows is the same as in Fig. 3.